Eur. Phys. J. Special Topics **227**, 921–932 (2018)

https://doi.org/10.1140/epjst/e2018-800019-1

THE EUROPEAN PHYSICAL JOURNAL SPECIAL TOPICS

Regular Article

Extreme events in epileptic EEG of rodents after ischemic stroke

A.N. Pisarchik[1,2,a], V.V. Grubov[1], V.A. Maksimenko[1], A. Lüttjohann[3], N.S. Frolov[1], C. Marqués-Pascual[2], D. Gonzalez-Nieto[2,4], M.V. Khramova[5], and A.E. Hramov[1]

[1] REC Artificial Intelligence Systems and Neurotechnologies, Yuri Gagarin State Technical University of Saratov, 410054 Saratov, Russia
[2] Center for Biomedical Technology, Technical University of Madrid, Campus Montegancedo, 28223 Pozuelo de Alarcon, Madrid, Spain
[3] Institute of Physiology I, University of Münster, Robert-Koch-Str 27a, 48149, Münster, Germany
[4] Biomedical Research Networking Center in Bioengineering Biomaterials and Nanomedicine (CIBER-BBN), Madrid, Spain
[5] Faculty of Computer Science and Information Technology, Saratov State University, 410012 Saratov, Russia

Received 13 February 2018
Published online 19 October 2018

Abstract. Extreme events are observed on electroencephalographic (EEG) recordings of rodents with induced ischemic stroke. These events represent themselves as post-stroke epileptic seizures in the form of spontaneous high-amplitude oscillations, which appear during the first 2–3 h after induced focal cerebral ischemia. The analysis of the EEG time-frequency structure reveals these extreme events as a sharp sudden growth of the wavelet energy in a particular frequency band, while the energy in the resting part of the power spectrum remains normal. The distinguished features of the extreme events are used for detection and quantification of the pathological brain activity.

1 Introduction

In recent years, a great attention of interdisciplinary scientific community has been devoted to the understanding of sudden abnormal deviations of a nonlinear dynamical system from its normal behavior, so-called extreme events [1,2]. Such interest is mainly caused by a high importance and economical benefits of the prediction of this kind of events in natural systems, such as rogue waves in the ocean [3], financial crush in stock market [4], and, as we will show in this paper, pathological brain states.

In dynamical systems, a typical time scale reflecting the system behavior outside an equilibrium state is defined by periods when a relevant variable undergoes small variations around some level determined by its long-time average [5,6]. In such systems, a sudden transition to a state where a dynamical variable significantly exceeds its long-time average is called *extreme event* [6]. Extreme events, initially associated

[a] e-mail: alexander.pisarchik@ctb.upm.es

with sudden changes in climate systems [7–9], financial systems [10,11], and social systems [12–14], nowadays are actively studied in physical systems, in particular, in quantum optics [15] and lasers [16–18], as well as in complex networks [19].

In model systems, the study of extreme events is mainly aimed at understanding the nature of this phenomenon and revealing its underlying mechanisms, which vary from one system to another. For instance, in the complex Ginzburg–Landau equation, the finite dissipation results in generation of incoherent background of interacting waves, which occasionally initiate large amplitude oscillations considered as extreme events [20]. Recently, extreme events were studied in the system of coupled FitzHugh–Nagumo oscillators [21–23], where, as was shown, they were induced by delayed coupling. Another type of extreme events was observed in a multistable Liénard system, where the underlying mechanisms were associated with interior crisis and intermittency [24].

The experimental evidence of extreme events was demonstrated in many systems. For example, in a spatially extended microcavity laser [6,18], a correlation between extreme events and the emergence of spatiotemporal chaos was detected. The mechanism of the observed behavior was shown to be related to quasiperiodic extended spatiotemporal intermittency. Other mechanisms of extreme events, associated with discontinuous boundaries and multistability were found in optically injected semiconductor [17], loss-modulated CO_2 [25], and pump-modulated fiber [16] lasers. Different approaches to the analysis of extreme events in big data were applied in ecosystems [26], climatic systems [27], population dynamics [28], etc. In the mentioned systems, the time series analysis allowed estimating main features of the observed extreme events and revealing mechanisms for their emergence.

In the complex network theory, a study of extreme events is inspired by the presence of such type of real-world networks behavior as traffic jams and other transportation networks, floods in the network of rivers, power blackouts due to the tripping of power grids, and spontaneous bursting activity in neuronal populations [29]. In addition, extreme events were studied in the network of FitzHugh–Nagumo oscillators [19,30], where the influence of the system size and the network topology on the extreme events generation was analyzed.

The huge diversity of extreme events and their underlying mechanisms allow us to expect the occurrence of such events in living systems, e.g., in neurophysiological brain activity. Actually, the fast development of migraine attacks and epileptic seizures caused by a sudden synchronization of billions of neurons exhibits dynamics similar to extreme events, demonstrating some properties of on-off intermittency [31–33]. The observed analogy makes it possible to describe the mechanisms that rule the generation of the extreme events in the brain neuronal network by considering neuron-based mathematical models. In this context, Ansmann et al. [34] described fundamental principles of extreme event generation in a "small-world" network, which can also be extended to other systems, e.g., excitation patterns in the heart or in the brain.

While in many fields of study, extreme event features were effectively revealed via time series analysis and described in many papers, extreme events in neurophysiological data, naturally generated by brain neurons, have not been yet considered. We expect that the application of the extreme event theory, along with traditional methods of electroencephalographic (EEG) analysis, may improve early diagnostics and control the development of brain pathologies, in particular, epileptic seizures [35]. This is a relevant task in the context of widely developed techniques aimed at prediction and analysis of brain seizure occurrence [36,37].

According to the above speculation, in this work, we observe and analyze a specific type of extreme events occurring in the mouse's brain after induced ischemic stroke, i.e., post-stroke seizures. We consider the time-frequency structure of EEG signals associated with extreme events. We show that this extreme behavior manifests itself

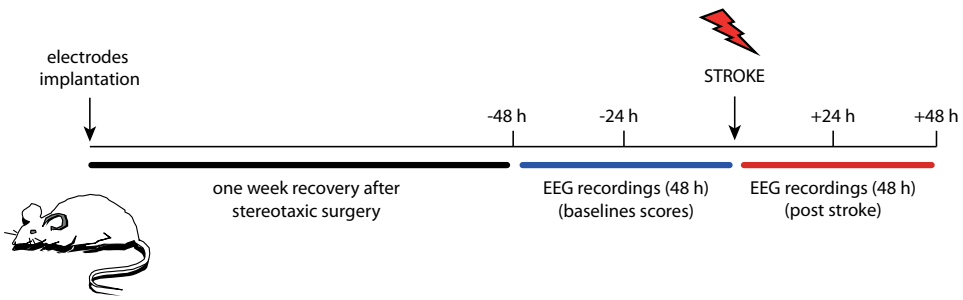

Fig. 1. Scheme of the experimental procedure divided in corresponding stages. The procedure started with the electrode implantation and post-surgery recovery period (marked in black). Afterwards, a recording of the baseline EEG was performed during the 48 h preceding the stroke (marked in blue). The post-stroke EEG was recorded during the next 48 h after the induced ischemic stroke (marked in red).

as a sharp sudden increase in the oscillation energy of a particular frequency band, while the dynamics in other bands remains almost unchanged. Based on the revealed features, we propose a novel method for the quantification of extreme events. We also validate our approach with EEG recordings related to normal and pathological brain activity, based on the time-frequency (wavelet) representation of the EEG signal.

2 Experimental procedure

2.1 Experimental design

In the present work, we analyzed EEG signals obtained from CD-1 mice after induced stroke. The experimental procedure was as follows. CD-1 mice were implanted with epidural electrodes (stereotaxic surgery) at frontal and parietal cortex of the left hemisphere. After one week, EEG recordings were performed during 48 consecutive hours to obtain baseline scores. After that, the mice were submitted to ischemic stroke by permanent occlusion of the middle cerebral artery (MCA), causing an unilateral infarction in the right hemisphere. Post-stroke EEG recordings from the left non-infarcted hemisphere were obtained during 48 h after the MCA occlusion. The experimental procedure showing all stages is illustrated in Figure 1. This experimental procedure was applied to all mice, but stroke was not induced in healthy mice.

To minimize 50-Hz electrical line interference, the EEG signal was filtered online through notch filter stop band, available on the EEG amplifier (Grass model 78D), which was able to reduce only a narrow band close to 50 Hz. In addition, the EEG signal was also acquired using electrical shielded cables to reduce noise effect. Although the notch filter can attenuate other frequencies nearby 50 Hz, this filter has almost no effect in the frequency ranges analyzed in this study.

2.2 Animals

Adult male CD-1 mice (25–35 g body weight; 3–8 weeks old) were bred and housed in the animal facility of the Center for Biomedical Technology. Six healthy and six post-stroke mice were used in our experimental stroke model. The animals were housed in individual cages with free access to food and water in an animal room with a controlled temperature and a natural light cycle. Daily routines were performed between 7 a.m. and 4 p.m. by authorized personnel. All procedures were approved by the

Ethical Committee for Animal Research of the Technical University of Madrid under Spanish Regulations for animal experimentation (Law 53/2013) and the Community of Madrid authorization (PROEX 393/15).

2.3 Electrophysiology

Electroencephalogram (EEG) recordings were performed as described in reference [38] with minor modifications. The mice were anesthetized with ketamine (100 mg/kg) and xylazine (10 mg/kg). During anesthesia the skull was exposed and three small holes were drilled over the cortex. EEG recordings were made using stainless-steel screw-electrodes (Plastics One, Virginia, USA). Two electrodes were fixed permanently into the skull in the frontal (from bregma: anterior +2.0 mm; laterally +1.7 mm) and parietal (from bregma: posterior −2.0 mm; laterally +1.7 mm) bones of the left hemisphere. The caudal electrode was placed in the parietal cortex, overlaying the dorsal hippocampus to capture EEG theta oscillations. The frontal electrode was placed over the frontal cortex to preferably capture EEG slow waves. A third electrode placed over the occipital cortex of the right hemisphere served as a ground electrode. The EEG signals were amplified by a Grass Model 78D polygraph, band-pass filtered (0.3–100 Hz) using a programmable signal conditioner (CyberAmp 380, Axon Instruments), and continuously sampled at 500 Hz using Labview software. It is worth mentioning that the recorded EEG voltage fluctuations resulted from the summarized ionic current within the brain, and therefore reflected collective dynamics of large groups of neurons [39], which makes it a suitable tool to measure brain seizure activity due to hypersynchrony.

2.4 Stroke model

Focal cerebral ischemia was induced in the right hemisphere by direct occlusion of the distal part of the right MCA as previously described in reference [40]. Mice were anesthetized with 2% isoflurane in air. A vertical skin incision (0.5 cm) was made between the right eye and the right ear under a dissection microscope and the temporal muscle was separated. The MCA was identified through the semitranslucent skull and a burr hole of a 0.8-mm diameter was made using a microdrill. After identification, the artery was ligated with a nylon ophthalmic suture (9–0) distally to the circle of Willis.

3 Signal analysis

We analyzed post-stroke mice EEG signals using the continuous wavelet transform [41,42]. The wavelet power spectrum $M(f,t) = |E(f,t)|^2$ was calculated for the whole EEG signal $X(t)$ in the range $f \in [1, 30]$ Hz. Here, the complex-value wavelet coefficients $E(f,t)$ are calculated as the convolution of analyzed signal $X(t)$ and a set of basic functions $\psi(f,t)$:

$$E(f,t) = \sqrt{f} \int_{t-4/f}^{t+4/f} X(t)\psi^*(f,t)dt, \tag{1}$$

where "*" marks complex conjugation. Each basic function from this set can be obtained from a function called *mother wavelet* as follows:

$$\psi(f,t) = \sqrt{f}\psi_0(f(t-t_0)), \tag{2}$$

where $f = 1/s$ (s being the time scale) defines the extension/compression of the mother wavelet and $(t - t_0)$ is the time shift of the mother wavelet.

In the present paper, we apply a complex Morlet wavelet often used for the analysis of neurophysiological data [41] as

$$\psi(f,t) = \pi^{1/4} \mathrm{e}^{j\omega_0 f(t-t_0)} \mathrm{e}^{(f(t-t_0))^2/2}, \tag{3}$$

where $\omega_0 = 2\pi$ is the central frequency of the Morlet mother wavelet function [43].

For single spectral component $f = f^*$, we used a normalized value of wavelet energy $W(f^*,t) = M(f^*,t)/M_{max}$, so that $W(f^*,t) \in [0,1]$. Here, M_{max} is the maximum wavelet energy across all frequencies in the range $f \in [1,30]$ Hz. Normalized wavelet energy distribution $W(f^*,t)$ was analyzed separately for each animal and for each frequency in the range $f \in [1,30]$ Hz. The analysis allowed us to find all maxima in wavelet energy distribution $W(f^*,t)$ and construct amplitude distributions of these maxima. We plotted the probability density function (PDF) of a given wavelet energy amplitude F, as histograms with a linear-scaled X axis ($W(f^*,t) \in [0,1]$) and a log-scaled Y axis (F). We found that during normal activity without epileptic discharges, empirical distribution $F(W)$ perfectly fits the Weibull distribution (see details in Sect. 4):

$$F_W(W|a,b) = \frac{b}{a}\left(\frac{W}{a}\right)^{b-1} \exp\left(-\left(\frac{W}{a}\right)^b\right), \tag{4}$$

where a and b are the parameters of Weibull distribution optimized to fit empirical PDF $F(W)$. At the same time, according to the extreme value theory, namely, the Pickands–Balkema–de Haan theorem [44,45], the exceeding tails of the empirical probability distribution function $F(W)$ (W surpasses threshold value W_δ) are modeled by the generalized Pareto distribution (GPD) [46,47]:

$$F_{\mathrm{GPD}}(W|k,\sigma,\theta) = \frac{1}{\sigma}\left(1 + k\frac{W-\theta}{\sigma}\right)^{-1-\frac{1}{k}}, \tag{5}$$

where k, σ, θ are the GPD parameters optimized to fit the exceeding tail of empirical probability distribution function $F(W)$. It should be noted, that W_δ is determined as an intersection point of the Weibull and GPD distribution curves.

In order to detect and quantify the degree of extreme behavior in the mouse's brain, we introduce the extreme event measure (EEM) defined as follows:

$$\mathrm{EEM} = \int_{W_\delta}^{1} |F(W) - F_W(W)|\, W dW. \tag{6}$$

EEM is a non-negative measure, close to zero for non-extremal (ordinary) dynamics, that increases in the presence of extreme events. Calculating EEM over the whole frequency range $f \in [1,30]$ Hz and comparing EEMs for different frequencies allowed us to find extreme events localized in certain frequency ranges.

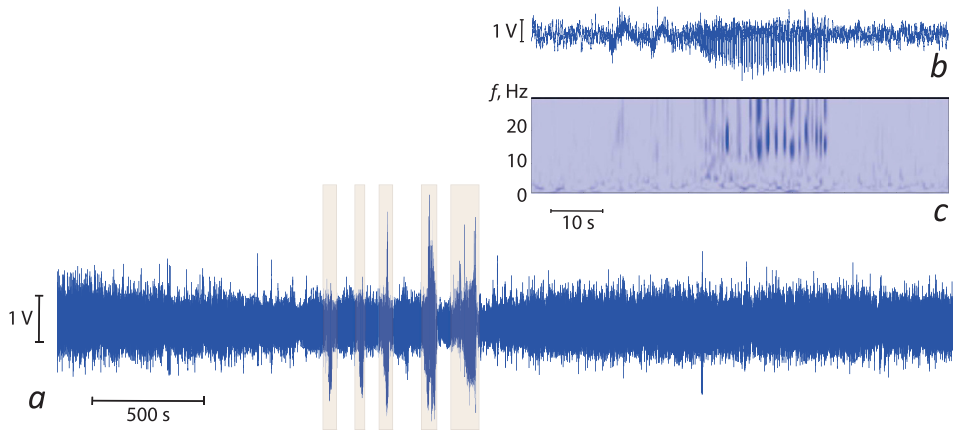

Fig. 2. Illustration of typical post-stroke seizures in mouse's EEG. (a) EEG signal recorded from mouse's brain during the first 2 h after induced stroke and amplified by factor 100. One can clearly observe the sequence of seizures in post-stroke mouse's brain activity (marked by shadow). (b) EEG fragment showing a single seizure and (c) corresponding wavelet energy surface demonstrating the time-frequency structure of a single seizure. It is seen that a single post-stroke seizure is characterized by increasing EEG signal amplitude along with increasing wavelet energy in certain frequency ranges.

4 Results

An ischemic stroke is known to initiate spontaneous neural activation resulting in the formation of synchronous EEG patterns. In EEG, this type of brain activity is associated with a sequence of high-amplitude spikes forming synchronous neural bursts. Such patterns are common in neuroscience and mainly related to the development of another pathological brain activity (epileptic seizure). The relation of such a behavior to stroke, known as *post-stroke epilepsy*, along with animal models, was also reported in humans [48].

The mice stroke is restricted to the brain cortex, specifically the somatosensorial and motor areas, causing permanent damage in the right hemisphere, which has profound consequences not only for the functionality of the infarcted hemisphere, but also for the non-infarcted left hemisphere [40]. In our case, the epileptiform episodes only appeared during the first 2–3 h after stroke surgery and no evidence of epileptiform activity was observed in the rest of the time period analyzed (48 h), while the EEG signal in the non-epileptic period remained very regular. Because the definition of an extreme event relates with sudden abnormal deviations from a normal (regular) behavior, we consider that this term is appropriate in the context of abrupt epileptic episodes.

Typical post-stroke seizures observed in mice are shown in Figure 2, where we present the EEG recording obtained from the mouse's brain during the first hour after induced stroke. Several well-pronounced seizures can be clearly distinguished in Figure 2a. The EEG fragment with a single post-stroke seizure and the wavelet spectrum for this seizure are shown in Figures 2b and 2c, respectively. In Figure 2a one can see that epileptic seizures are characterized by a sharp increase in the EEG amplitude that significantly exceeds the long-time average. Such epochs of approximately 30-second duration appear spontaneously and in the same unpredictable manner. The sharp onset and offset are clearly seen in Figure 2b, where the individual seizure event is shown in detail. Unlike typical extreme events considered in model and real

systems, the observed seizure epochs are characterized by a relatively long duration when a dynamical variable describing the system state (action potential) varies within a large amplitude range. This is a common behavior of neurophysiological systems, where the neural ensemble involved in the generation of different rhythms, produces a macroscopic signal with complex spectral compound [39]. This means that the considered extreme events are complex patterns distributed in a time-frequency domain.

The time-frequency (wavelet) structure of a single seizure is shown in Figure 2c. One can see that despite the complex behavior within the pattern, it is strictly determined by certain spectral properties. In particular, spectral energy has sharp peaks in a certain frequency band, while in other bands the energy value behaves mostly homogeneously. It can be supposed that the extreme behavior in this system results from a sudden appearance (or disappearance) of a particular oscillatory mode. Therefore, in order to analyze extreme events of neural activity, one should specify spectral properties of this type of event. According to previous neurophysiological studies, an effective approach is based on the analysis of spectral energy components in different spectral regions. In particular, the analysis made for EEG signals of epileptic rats demonstrated the presence of various oscillatory patterns, such as absence seizures [49], their delta and theta precursors [50], non-epileptic sleep spindles, and 5−9 Hz oscillations [51]. According to these results, the energy band can be searched taking into account predefined properties of the analyzed oscillatory pattern or the well-known characteristic frequency bands: 1−4.5 Hz (delta), 5−8.5 Hz (theta), 9−13.5 Hz (alpha), 14−31.5 Hz (beta), 32−59.5 Hz (gamma 1), and 60−100 Hz (gamma 2) ranges.

In our study, the spectral band was chosen in the middle frequency range (15−30 Hz) according to the spectral properties of the considered extreme events (see Fig. 2c). It was supposed that the extreme behavior would represent itself as a sharp sudden increase in the wavelet energy in this particular band, while the neuronal dynamics in other bands would remain non-extreme.

In order to check this hypothesis, the EEG spectrum was calculated for 30 individual frequencies within the 1–30 Hz spectral band: $f_1 = 1$ Hz, $f_2 = 2$ Hz,..., $f_{30} = 30$ Hz. For each considered frequency, the values of wavelet energy $M(t)$ and normalized wavelet energy $W_n(t)$ $(n = 1,\ldots,30)$, i.e., $W_1(t) = W(f_1, t)$, $W_2(t) = W(f_2, t)$,..., $W_{30}(t) = W(f_{30}, t)$ were calculated from the EEG signal at every moment of time t. The local maxima of wavelet energy $W(t)$ were found and PDFs of these maxima $F(W)$ were constructed. The corresponding typical distributions (PDF) are shown in Figure 3a for the chosen frequency values: $f = 5$ Hz, $f = 10$ Hz, $f = 18$ Hz, and $f = 20$ Hz. One can see that for low frequency ($f = 5$ Hz), the PDF is accurately approximated by the Weibull distribution indicating non-extremal dynamics. As the frequency increases, the probability distribution function $F(W)$ exhibits an exceeding tail, which conforms the generalized Pareto distribution. According to the Pickands–Balkema–de Haan theorem [44,45], such a behavior can be called *extreme* behavior, if the amplitude of the wavelet spectrum in a certain frequency range exceeds the intersection point of the Weibull PDF and the generalized Pareto PDF. This additional part of distribution is more pronounced at higher frequencies and can be seen most clearly at $f = 20$ Hz. It should be noted that some points of $F(W)$ are outside the analytical (yellow) curve of the Weibull distribution even at small frequencies, i.e., at $f \leq 10$ Hz. However, the number of such points is insignificant and their occurrence is not determined by the extreme behavior; they are associated with the EEG recording quality.

To compare the significance of the additional part on the PDFs for different frequencies, we calculated the EEM frequency dependence in the range of 1–30 Hz, which typical shape can be seen in Figure 3b. This dependence reaches a maximum at $f = 20$ Hz. Since EEM is proportional to the area between the Weibull distribution

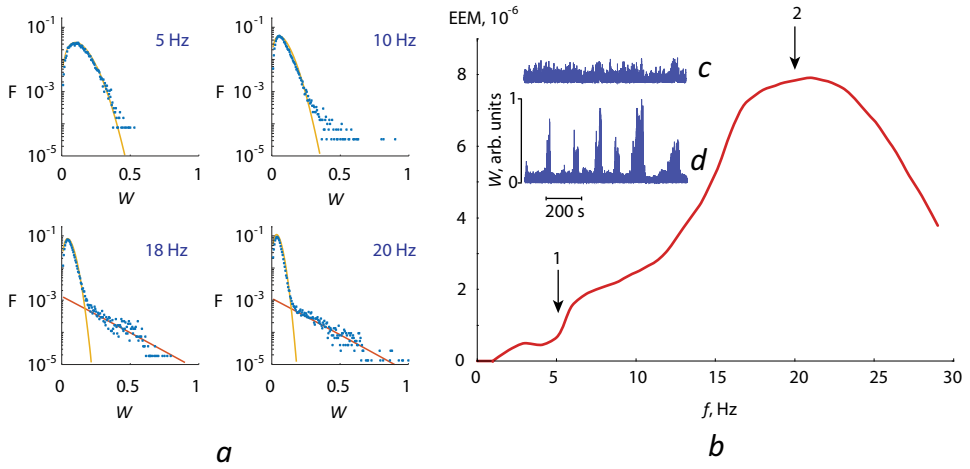

Fig. 3. Results of statistical analysis provided for individual mouse recordings. (a) Distributions of wavelet energy amplitudes for frequencies $f = 5$ Hz, $f = 10$ Hz, $f = 18$ Hz and $f = 20$ Hz. Here, the blue dots correspond to empirical probability distribution function $F(W)$, the yellow curve of Weibull distribution fits non-extreme part of $F(W)$, while the red straight line of GPD fits extreme part of $F(W)$. (b) Extreme event measure (EEM) frequency dependence in the range of 1–30 Hz. "1" and "2" highlight points belonging to non-extreme and extreme behaviors, respectively. (c,d) Time series of normalized wavelet energy $W(t)$ for $f = 5$ Hz and $f = 20$ Hz, respectively. It can be seen that post-stroke extreme behavior is perfectly fitted by GPD and mostly pronounced at high frequencies (15–25 Hz).

curve and the empirical PDF $F(W)$ for $W \geq W_\delta$, we assume that high EEM values are associated with extreme events. In particular, we examined two specific frequencies in the EEM frequency dependence, marked in Figure 3b by the arrows at $f = 5$ Hz (1) and $f = 20$ Hz (2). The corresponding time series of the normalized wavelet energy $W(t)$ are shown in Figures 3c (frequency 1) and 3d (frequency 2). It is clearly seen that the time series corresponding to "frequency 2" exhibits a number of well-pronounced extreme pulses, while the time series corresponding to "frequency 1" looks normal.

To prove that the observed extreme events are related to seizures and post-stroke EEG activity, we carried out the analysis of the EEG signals for two types of mice: mice with post-stroke epileptic seizures and mice without epilepsy. For these two groups of mice, we performed the same analysis as for the mouse in Figure 3 and then compared the results. Figure 4 illustrates the results obtained for 6 healthy and 6 post-stroke mice.

Figure 4a shows wavelet energy amplitude PDFs for frequencies $f = 5$ Hz and $f = 20$ Hz for healthy (marked in red) and post-stroke (marked in blue) mice. For comparison, the overlapped distributions are plotted in the right column of Figure 4a. One can see that at frequency $f = 5$ Hz these two distributions are quite similar. However, the situation is a bit different at frequency $f = 20$ Hz, where one can clearly see that the PDF of the post-stroke mouse unusually increases in the area of higher values of W. As we proposed earlier, such an increase indicates the presence of extreme events, whereas the corresponding PDF for a healthy mouse lacks it. We also calculated the EEM frequency dependencies for two groups of mice, 6 healthy and 6 post-stroke mice, shown in Figure 4b. It is obvious, that EEMs for post-stroke mice demonstrate a well-pronounced maximum at $f = 22$–24 Hz associated with the emergence of extreme events (see Fig. 3b). It is also clear that the EEM frequency

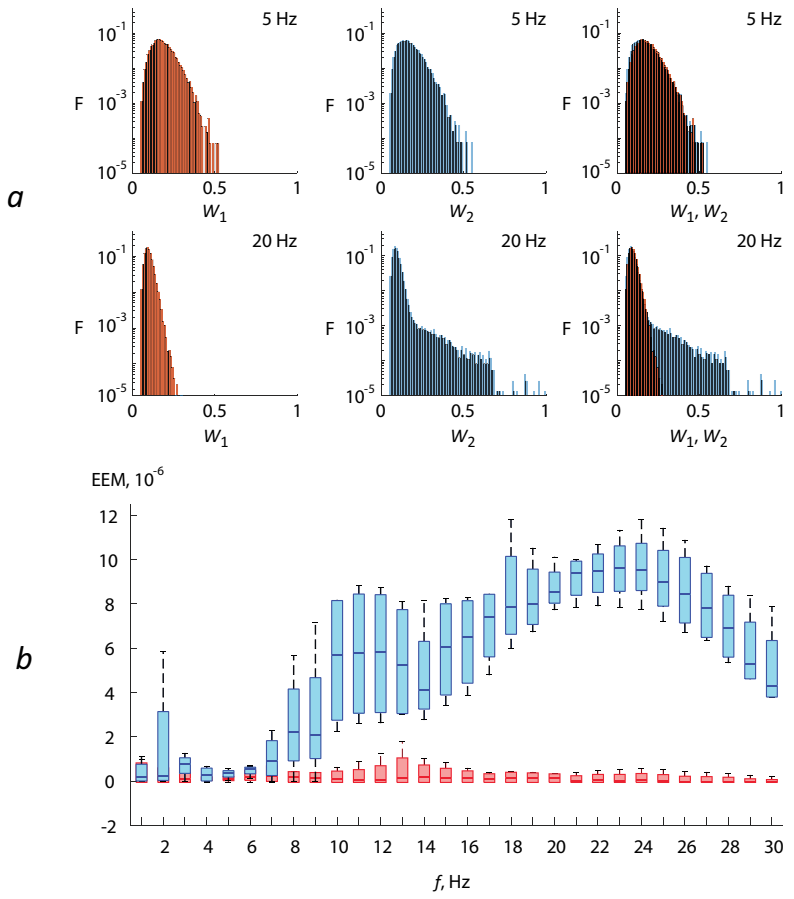

Fig. 4. Results of statistical analysis for two groups of mice: mice with stroke and healthy mice. (a) Left column: distributions of wavelet energy amplitudes at frequencies $f = 5$ Hz and $f = 20$ Hz for a healthy mouse (marked in red); middle column: distributions of wavelet energy amplitudes at $f = 5$ Hz and $f = 20$ Hz for a mouse with stroke (marked in blue); right column: overlapped distributions of wavelet energy amplitudes for both healthy and post-stroke mice for better visualization. (b) Box-and-whiskers plot of EEM versus frequency for 6 healthy mice (colored in red) and 6 mice with stroke (colored in blue). One can see the pronounced difference in post-stroke and healthy mice brain behavior by comparing the introduced statistical measures. Moreover, EEM allows the localization of a frequency band characterized by extreme brain behavior (10–30 Hz) with maximum at 22–24 Hz.

dependences for the healthy group are close to zero within the considered frequency band and do not have pronounced maxima.

It should be noted that in the electrophysiological configuration used in this study (low impedance electrodes placed over the cortical brain surface), the electrocorticogram signal acquired in the animals is mostly associated with the activity of subthreshold post-synaptic potentials (extracellular fields derived from transmembrane currents) from different neuronal networks (no isolate neuron), since at the used filtering frequency (0.3–100 Hz) and sample frequency (500 Hz) the action potentials do not contribute substantially to the EEG signal or electrocorticogram band (<100 Hz). In addition, gap junctions also indirectly participate in extracellular fields recorded from brain surface, although gap junctions permit an ionic transfer between neural cells by modulating neuronal excibitability.

Although a significant proportion of patients and animals have EEG seizures in the acute phase of stroke or other forms of brain damage (for example, traumatic brain injury), across the literature the exact mechanisms underlying epilepsy after stroke remain elusive. It was hypothesized that in the first hours after stroke, neuronal networks within the ischemic penumbra (peri-lesional cortex, surrounding the infarct core) may be capable of initiating post-stroke epileptogenesis. In our study, seizures occurred exclusively during the first 2–3 h after stroke in an interval of 48 h of analysis (post-stroke). However, recurring seizures were also found in humans and animals longer after stroke, which is probably related with progressive molecular and cellular events (for example, neurogenesis, synaptic plasticity, epigenetic, oxidation) leading to structural and functional changes in neuronal networks. Complex changes in neuronal excitability (hyper-excitability) were also proposed to occur in both hemispheres (the infarcted and non-infarcted) and might account for the recurring seizures occurring in later stages after brain stroke. However, as suggested in previous stroke studies, during the acute phase of stroke (our study), hypoxia and metabolic dysfunction, glutamate excitotoxicity and local GABAergic signalling inhibition (which translates into desinhibition) might tentatively be responsible for the abrupt epileptic episodes observed.

5 Conclusions

In this paper, we have shown that epileptic seizures observed in the EEG recordings of rodents after an induced ischemic stroke, behave as extreme events. In the considered case, the artificially induced ischemic stroke resulted in a change in the mice brain activity. The post-stroke mice demonstrated a sequence of seizures during a rather long time interval, and, afterward, returned to their normal activity. In our study, we focused on the investigation of statistical properties of the post-stroke mice behavior from the viewpoint of the extreme value theory (EVT), rather than a simple detection of seizures in the EEG time series. These events manifested themselves as spontaneous high-amplitude oscillations, which appeared during the first 2–3 h after induced focal cerebral ischemia. The wavelet analysis of the EEG signals corresponding to the observed extreme events revealed a sharp sudden increase in the wavelet energy in a particular spectral range corresponding to epileptic seizure activity, while the energy at other frequencies remained almost unchanged. The identified distinguished features allowed us to develop a novel method for detection and quantification of extreme events in EEG recordings associated with pathological brain activity.

The proposed statistical approach to pathological EEG analysis could be further developed for detection and prediction of abnormal brain activity caused by ischemic stroke. This is an actual and, at the same time, an open problem, which has several other possible solutions. For example, one can use the properties of well-known models uncovered via bifurcation analysis to develop a criteria for post-stroke seizure prediction [52,53]. We believe that the developed method can be useful not only for detecting epileptic seizures, but also for diagnosing and predicting other abnormalities in the central nervous system.

The authors thank Soledad Martinez–Murillo for technical assistance in performing experiments. This work has been supported by the Ministry of Education and Science of Russian Federation (grant 3.861.2017/4.6) and President Program (projects NSH-2737.2018.2). A.N.P. acknowledges individual support from the Ministry of Economy and Competitiveness (Spain) (project SAF2016-80240). D.G.N. acknowledges individual support from the Community of Madrid (grant Neurocentro-B2017/BMD-3760). A.E.H. acknowledges individual support from the Ministry of Education and Science of Russian Federation (project 3.4593.2017/6.7).

References

1. S. Albeverio, V. Jentsch, H. Kantz, *Extreme Events in Nature and Society* (Springer-Verlag, Berlin, Heidelberg, 2006)
2. J.H. Wu, Q. Jia, Sci. Rep. **6**, 21612 (2016)
3. D.I. Yeom, B.J. Eggleton, Nature **450**, 953 (2007)
4. P. Piccoli, M. Chaudhury, A. Souza, Res. Int. Bus. Financ. **42**, 275 (2017)
5. G. Nicolis, C. Nicolis, *Foundations of Complex Systems: Emergence, Information, and Predicition* (World Scientific, Singapore, 2012)
6. S. Coulibaly, M.G. Clerc, F. Selmi, S. Barbay, Phys. Rev. A **95**, 023816 (2017)
7. O. Mazdiyasni, A. AghaKouchak, Proc. Natl. Acad. Sci. **112**, 11484 (2015)
8. N.S. Diffenbaugh, J.S. Pal, R.J. Trapp, F. Giorgi, Proc. Natl. Acad. Sci. **102**, 15774 (2005)
9. N. Marwan, J. Kurths, Chaos **25**, 097609 (2015)
10. J. Anttila-Hughes, Europ. Phys. J. Special Topics **225**, 527 (2016)
11. W. Gan-Hua, Q. Lu, M. Stephen, L. Xin-Li, Y. Yue, Y. Hui-Jie, J. Yan, Chin. Phys. B **23**, 128901 (2014)
12. D. Helbing et al., J. Stat. Phys. **158**, 735 (2015)
13. J.M. Miotto, E.G. Altmann, PLoS One **9**, 1 (2014)
14. S. Stieglitz, D. Bunker, M. Mirbabaie, C. Ehnis, J. Conting. Crisis Manag. **26**, 4 (2018)
15. C. Aghamohammadi, S.P. Loomis, J.R. Mahoney, J.P. Crutchfield, Phys. Rev. X **8**, 011025 (2018)
16. A.N. Pisarchik, R. Jaimes-Reátegui, R. Sevilla-Escoboza, G. Huerta-Cuellar, M. Taki, Phys. Rev. Lett. **107**, 274101 (2011)
17. J. Zamora-Munt, B. Garbin, S. Barland, M. Giudici, J.R.R. Leite, C. Masoller, J.R. Tredicce, Phys. Rev. A **87**, 035802 (2013)
18. F. Selmi, S. Coulibaly, Z. Loghmari, I. Sagnes, G. Beaudoin, M.G. Clerc, S. Barbay, Phys. Rev. Lett. **116**, 013901 (2016)
19. R. Karnatak, G. Ansmann, U. Feudel, K. Lehnertz, Phys. Rev. E **90**, 022917 (2014)
20. J.W. Kim, E. Ott, Phys. Rev. E **67**, 026203 (2003)
21. X. Sun, J. Lei, M. Perc, J. Kurths, G. Chen, Chaos **21**, 016110 (2011)
22. Q. Wang, G. Chen, M. Perc, PLoS One **6**, e15851 (2011)
23. A. Saha, U. Feudel, Phys. Rev. E **95**, 062219 (2017)
24. S.L. Kingston, K. Thamilmaran, P. Pal, U. Feudel, S.K. Dana, Phys. Rev. E **96**, 052204 (2017)
25. C. Bonatto, A. Endler, Phys. Rev. E **96**, 012216 (2017)
26. R.D. Batt, S.R. Carpenter, A.R. Ives, Limnol. Oceanogr. Lett. **2**, 63 (2017)
27. J.F. Mitchell, J. Lowe, R.A. Wood, M. Vellinga, Philos. Trans. R. Soc. Lond. A **364**, 2117 (2006)
28. B. Dennis, R. Desharnais, J. Cushing, S. Henson, R. Costantino, Ecol. Monogr. **71**, 277 (2001)
29. V. Kishore, M.S. Santhanam, R.E. Amritkar, Phys. Rev. Lett. **106**, 188701 (2011)
30. G. Ansmann, R. Karnatak, K. Lehnertz, U. Feudel, Phys. Rev. E **88**, 052911 (2013)
31. A.E. Hramov, A.A. Koronovskii, I.S. Midzyanovskaya, E. Sitnikova, C.M. Rijn, Chaos **16**, 043111 (2006)
32. E. Sitnikova, A.E. Hramov, V.V. Grubov, A.A. Ovchinnkov, A.A. Koronovsky, Brain Res. **1436**, 147 (2012)
33. A.A. Koronovskii, A.E. Hramov, V.V. Grubov, O.I. Moskalenko, E. Sitnikova, A.N. Pavlov, Phys. Rev. E **93**, 032220 (2016)
34. G. Ansmann, K. Lehnertz, U. Feudel, Phys. Rev. X **6**, 011030 (2016)
35. G. Luijtelaar van, A. Luttjohann, V.V. Makarov, V.A. Maksimenko, A.A. Koronovskii, A.E. Hramov, J. Neurosci. Meth. **260**, 144 (2016)
36. S. Panahi, Z. Aram, S. Jafari, J. Ma, J. Sprott, Chaos Soliton. Fract. **105**, 150 (2017)
37. Z. Aram, S. Jafari, J. Ma, J.C. Sprott, S. Zendehrouh, V.T. Pham, Commun. Nonlin. Sci. Num. Simul. **44**, 449 (2017)

38. L. Fernández-García, N. Marí-Buyé, J.A. Barios, R. Madurga, M. Elices, J. Pérez-Rigueiro, M. Ramos, G.V. Guinea, D. González-Nieto, Acta Biomater. **45**, 262 (2016)
39. V.A. Maksimenko, A. Lüttjohann, V.V. Makarov, M.V. Goremyko, A.A. Koronovskii, V. Nedaivozov, A.E. Runnova, G. van Luijtelaar, A.E. Hramov, S. Boccaletti, Phys. Rev. E **96**, 012316 (2017)
40. J.A. Barios, L. Pisarchyk, L. Fernandez-Garcia, L.C. Barrio, M. Ramos, R. Martinez-Murillo, D. Gonzalez-Nieto, J. Cerebr. Blood Flow Metab. **36**, 606 (2016)
41. A.N. Pavlov, A.E. Hramov, A.A. Koronovskii, Y.E. Sitnikova, V.A. Makarov, A.A. Ovchinnikov, Physics-Uspekhi **55**, 845 (2012)
42. A.E. Hramov, A.A. Koronovskii, V.A. Makarov, A.N. Pavlov, E. Sitnikova, *Wavelets in Neuroscience*, Springer Series in Synergetics (Springer, Heidelberg, 2015)
43. E. Sitnikova, A.E. Hramov, V. Grubov, A.A. Koronovsky, Brain Res. **1543**, 290 (2014)
44. A.A. Balkema, L. De Haan, Ann. Probab. **2**, 792 (1974)
45. J. Pickands, Ann. Stat. **3**, 119 (1975)
46. J.R. Hosking, J.R. Wallis, Technometrics **29**, 339 (1987)
47. V. Pisarenko, D. Sornette, Pure Appl. Geophys. **160**, 2343 (2003)
48. P.K. Myint, E.F.A. Staufenberg, K. Sabanathan, Postgrad. Med. J. **82**, 568 (2006)
49. V.A. Maksimenko, S. van Heukelum, V.V. Makarov, J. Kelderhuis, A. Lüttjohann, A.A. Koronovskii, A.E. Hramov, G. van Luijtelaar, Sci. Rep. **7**, 2487 (2017)
50. G. van Luijtelaar, A. Hramov, E. Sitnikova, A. Koronovskii, Clin. Neurophysiol. **122**, 687 (2011)
51. E. Sitnikova, A.E. Hramov, A.A. Koronovsky, G. van Luijtelaar, J. Neurosci. Meth. **180**, 304 (2009)
52. J. Ma, J. Tang, Nonlin. Dyn. **89**, 1569 (2017)
53. C. Wang, J. Ma, Int. J. Mod. Phys. B **32**, 1830003 (2018)